

# Cation-Size-Mismatch Tuning of Photoluminescence in Oxynitride Phosphors

Wei-Ting Chen,<sup>†</sup> Hwo-Shuenn Sheu,<sup>‡</sup> Ru-Shi Liu,<sup>\*,†</sup> and J. Paul Attfield<sup>\*,§</sup>

<sup>†</sup>Department of Chemistry, National Taiwan University, Taipei 106, Taiwan

<sup>‡</sup>National Synchrotron Radiation Research Center, Hsinchu 300, Taiwan

<sup>§</sup>Centre for Science at Extreme Conditions and School of Chemistry, University of Edinburgh, King's Buildings, Mayfield Road, EH9 3JZ Edinburgh, U.K.

**S** Supporting Information

**ABSTRACT:** Red or yellow phosphors excited by a blue light-emitting diode are an efficient source of white light for everyday applications. Many solid oxides and nitrides, particularly silicon nitride-based materials such as  $M_2Si_5N_8$  and  $MSi_2O_2N_2$  ( $M = Ca, Sr, Ba$ ),  $CaAlSiN_3$ , and  $SiAlON$ , are useful phosphor hosts with good thermal stabilities. Both oxide/nitride and various cation substitutions are commonly used to shift the emission spectrum and optimize luminescent properties, but the underlying mechanisms are not always clear. Here we show that size-mismatch between host and dopant cations tunes photoluminescence shifts systematically in  $M_{1.95}Eu_{0.05}Si_{5-x}Al_xN_{8-x}O_x$  lattices, leading to a red shift when the  $M = Ba$  and  $Sr$  host cations are larger than the  $Eu^{2+}$  dopant, but a blue shift when the  $M = Ca$  host is smaller. Size-mismatch tuning of thermal quenching is also observed. A local anion clustering mechanism in which  $Eu^{2+}$  gains excess nitride coordination in the  $M = Ba$  and  $Sr$  structures, but excess oxide in the  $Ca$  analogues, is proposed for these mismatch effects. This mechanism is predicted to be general to oxynitride materials and will be useful in tuning optical and other properties that are sensitive to local coordination environments.

The (oxo)nitridosilicates  $M_2Si_5N_8$  and  $MSi_2O_2N_2$  ( $M = Ca, Sr, Ba$ ) doped with  $Eu^{2+}$  are widely used as red phosphors to provide warm white light-emitting diode (LED) devices.<sup>1–9</sup> Intermediate materials made by substituting  $AlO^+$  for  $SiN^+$  in the  $M_2Si_5N_8$  family to create  $M_2Si_{5-x}Al_xN_{8-x}O_x$  SiAlONs (silicon aluminum oxide nitrides) are mentioned briefly in an early paper, but systematic substitutional effects on the photoluminescence were not reported.<sup>10</sup> We have prepared and characterized ceramic  $M_{1.95}Eu_{0.05}Si_{5-x}Al_xN_{8-x}O_x$  materials with a constant 2.5% doping of  $Eu^{2+}$  at the  $M^{2+}$  sites for  $M = Ca, Sr$ , and  $Ba$  up to the approximate solid solution limit of  $x = 1$ .

Smooth changes of lattice parameters with  $x$  in Figure 1a demonstrate that  $M_{1.95}Eu_{0.05}Si_{5-x}Al_xN_{8-x}O_x$  solid solutions are formed. The lattice expands with  $x$  for all three  $M$  cations, as expected for the replacement of  $SiN^+$  (sum of ionic radii  $^{[4]}r(Si^{4+}) + ^{[4]}r(N^{3-}) = 0.26 + 1.46 = 1.72 \text{ \AA}$ ; the leading bracketed superscript shows the coordination number throughout) by the slightly larger  $AlO^+$  combination ( $^{[4]}r(Al^{3+}) +$

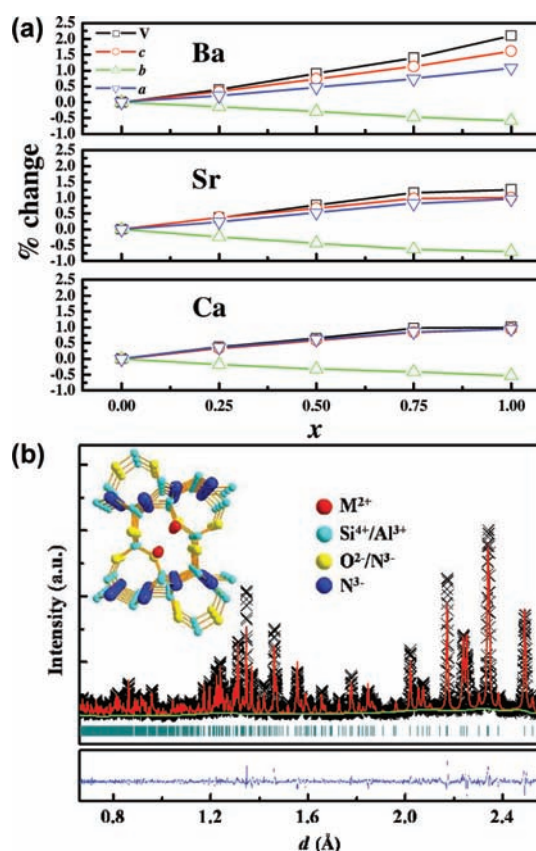


**Figure 1.** Structural results for  $M_{1.95}Eu_{0.05}Si_{5-x}Al_xN_{8-x}O_x$  ( $M = Ca, Sr, Ba$ ) materials. (a) Relative shifts in the lattice parameters with  $x$ . We use pseudo-orthorhombic parameters  $a = b_m, b = a_m/2, c = c_m$  for the monoclinic  $Ca$  series cells ( $m$  subscripts) for direct comparison with the orthorhombic  $M = Sr$  and  $Ba$  series. (b) Fit to time-of-flight neutron diffraction data for  $Ba_{1.95}Eu_{0.05}Si_4AlN_7O$ . Structure refinement shows that the oxygen atoms substitute only for  $^{[2]Si}N$  (nitrides bonded to two silicons), and not at  $^{[3Si]}N$  sites, as illustrated in the inset view of the crystal structure.

$^{[4]}r(O^{2-}) = 0.39 + 1.38 = 1.77 \text{ \AA}$ ).<sup>11</sup> The parent structures contain equal numbers of nitrides bonded to two or three silicon neighbors, as represented in the formula

Received: February 17, 2012

Published: April 26, 2012

$M_2Si_5^{[3Si]}N_4^{[2Si]}N_4$ . The anion distribution in a  $Ba_{1.95}Eu_{0.05}Si_4AlN_7O$  sample, determined from a neutron diffraction study (Figure 1b), shows that the oxygen atoms substitute only at  $^{[2Si]}N$  sites. This is consistent with oxosilicate chemistry, where  $^{[3Si]}O$  coordination is not observed, and illustrates the “Pauling’s second rule” model for anion distributions,<sup>12</sup> as the lower valent oxide anion is less coordinated by high-valent silicon. This partial anion order is important to the optical properties below, as the M cation sites are coordinated principally by the  $^{[2Si]}N/O$  anions.

Photoluminescence spectra of the  $M_{1.95}Eu_{0.05}Si_{5-x}Al_xN_{8-x}O_x$  materials are shown in Figure 2a. The peak emission wavelengths for the  $x = 0$  nitride materials are similar to

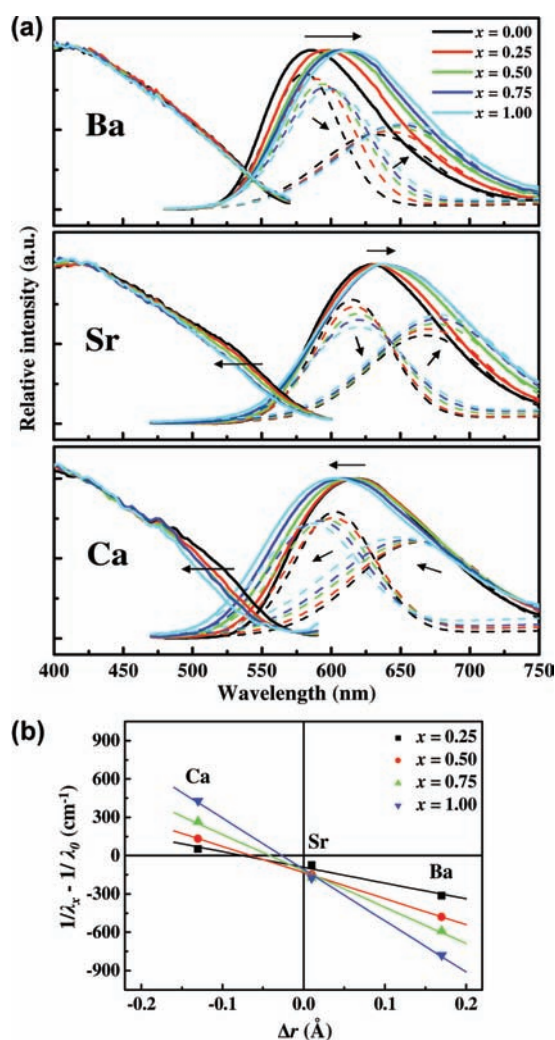


**Figure 2.** Photoluminescence of  $M_{1.95}Eu_{0.05}Si_{5-x}Al_xN_{8-x}O_x$  materials ( $M = Ca, Sr, Ba$ ). (a) Normalized excitation (lower wavelength contribution) and photoluminescence spectra from excitation by a Xe lamp at room temperature. The photoluminescence spectra are decomposed into Gaussian contributions from the two M cation sites in the  $M_2Si_5N_8$  type structures. The arrows illustrate the energy shift and change in relative intensity of the spectra with increasing  $x$ . (b) Graph showing the energy shift (in wavenumbers) for the peak photoluminescence of  $M_{1.95}Eu_{0.05}Si_{5-x}Al_xN_{8-x}O_x$  materials ( $M = Ca, Sr, Ba$ ) vs  $\Delta r = r(M^{2+}) - r(Eu^{2+})$ , the difference between ionic radii of the host (M) and dopant (Eu) cations, for several compositions  $x$ . The crossover of the constant composition lines near  $\Delta r = 0$  demonstrates the size-mismatch effect.

those reported previously<sup>8,13–15</sup> and are in the order  $Sr > Ca > Ba$ . This irregular sequence reflects a complex balance of lattice and local coordination effects, notably a change in crystal structure type between the  $M = Sr$  and  $Ca$  materials. A surprising observation is that the photoluminescence maximum shifts to longer wavelengths (a red shift) with increasing  $AlO^+$  substitution,  $x$ , in the  $M = Ba$  and  $Sr$  series, but a pronounced blue shift to shorter wavelengths is observed in the  $Ca$  analogues. This variation and switching of energy shift was not reported in studies of  $M_{2-y}Eu_ySi_5N_8$  and  $M_{1-y}Eu_ySi_2O_2N_2$ , where the emission wavelength shows a red shift with  $y$  reflecting typical Stokes and reabsorption effects in both series.<sup>8,9</sup> Our observed energy shifts for  $M = Ba, Sr$ , and  $Ca$  samples display a size-mismatch variation. The host  $M = Ba, Sr$ , and  $Ca$  cations show a significant dispersion of sizes ( $^{[8]}r(M^{2+}) = 1.42, 1.26, \text{ and } 1.12 \text{ \AA}$  respectively), and the europium dopant ( $^{[8]}r(Eu^{2+}) = 1.25 \text{ \AA}$ ) is slightly smaller than  $Sr^{2+}$ . A red shift is observed for  $M = Ba$  and  $Sr$  hosts larger than the emitting dopant  $Eu^{2+}$  ions, but for smaller  $Ca^{2+}$  cations this switches to a blue shift. Plotting the energy shifts against the size difference  $\Delta r = r(M^{2+}) - r(Eu^{2+})$  for each set of three samples with the same  $x$  gives a series of lines that cross near  $\Delta r = 0$  (Figure 2b), showing that the shifts have an approximately linear dependence on size-mismatch.

A strong size-mismatch influence on thermal quenching of photoluminescence, which is important to the performance of white-LED devices, is also observed in the  $M_{1.95}Eu_{0.05}Si_{5-x}Al_xN_{8-x}O_x$  materials, as shown in Figure 3. The onset temperature for thermal quenching remains at  $\sim 300$  K for the  $M = Sr$  and  $Ba$  series as the level of  $AlO^+$  substitution increases up to  $x = 1$ , but decreases to  $\sim 150$  K for  $M = Ca$  materials. The undoped  $x = 0$  materials all have quenching activation energies  $\sim 0.28$  eV, but the values for the three series diverge with increasing  $x$  (Figure 3b). The activation energy rises slightly in the  $Ba$  series but is suppressed to 0.10 eV at  $x = 1$  for  $M = Ca$ .

Systematic changes in  $Eu^{2+}$  populations at the two distinctive  $M^{2+}$  sites with different coordination environments in the  $M_2Si_5N_8$  crystal structures were investigated as a possible origin of the above size-mismatch effects.<sup>16</sup> Figure 2a shows that photoluminescence intensity is transferred from the shorter wavelength (higher coordination M-site) component to the longer wavelength (less coordinated site) peak with increasing  $x$  in all three  $M_{1.95}Eu_{0.05}Si_{5-x}Al_xN_{8-x}O_x$  series. This increase in nonradiative crossing is supported by time-resolved photoluminescence spectra shown in Supporting Information, but the time-dependent energy shifts and the crossing rates do not correlate with  $\Delta r$ , so the size-mismatch variations in Figures 2 and 3 are not attributable to changes of relative  $Eu^{2+}$  site populations.

To explain the size-mismatch variations of energy shift and thermal quenching with  $x$  in  $M_{1.95}Eu_{0.05}Si_{5-x}Al_xN_{8-x}O_x$  phosphors, we propose a model based on changes in the local numbers of nitride and oxide anions coordinated to  $Eu^{2+}$ . These changes tune the photoluminescence energy by altering the balance between two competing effects. The lattice and the  $Eu^{2+}$  coordination environments expand with  $x$ , as  $AlO^+$  is slightly larger than  $SiN^+$ , resulting in a red shift. However, the partial substitution of oxide for nitride coordinated to  $Eu^{2+}$  leads to a blue shift with  $x$  through changes in crystal field and nephelauxetic effects. The net outcome in an ideal, cation-size-matched  $M_{1.95}Eu_{0.05}Si_{5-x}Al_xN_{8-x}O_x$  series turns out to be a small red shift, as evidenced by the energy offsets of the lines in

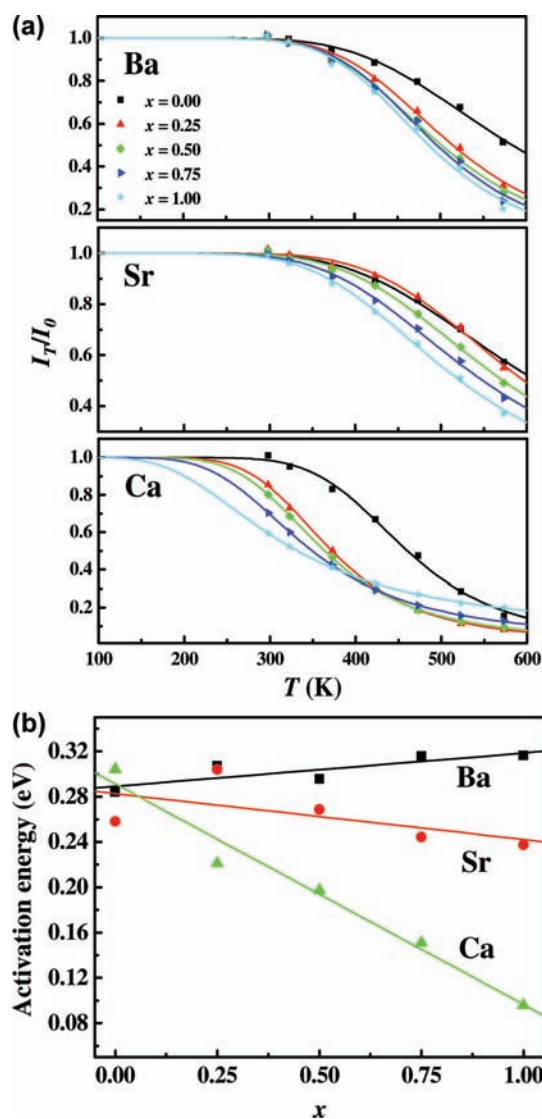


**Figure 3.** Thermal quenching of photoluminescence for  $M_{1.95}Eu_{0.05}Si_{5-x}Al_xN_{8-x}O_x$  materials ( $M = Ca, Sr, Ba$ ). (a) Photoluminescence intensity ratios  $I_T/I_0$  measured at temperatures  $T = 298 - 573$  K. The curves show fits of the equation  $I_T/I_0 = [1 + D \exp(-E_a/kT)]^{-1}$ , where  $I_0$  (the intensity at  $T = 0$ ),  $D$ , and the activation energy  $E_a$  were refined variables. (b) Plot of the activation energies against composition variable  $x$  for the  $M = Ca, Sr,$  and  $Ba$  series showing a size-mismatch variation of the slopes.

Figure 2b at  $\Delta r = 0$  (and the  $M = Sr$  series data where the size-mismatch is small). In this ideal structure, the average numbers of oxide and nitride anions coordinated to  $Eu^{2+}$  would be the same as the overall structural average for the  $M^{2+}$  cations. However, the local  $Eu^{2+}$  coordination changes when a large mismatch is present through a simple size-compensation mechanism as the difference between anion radii ( $[^{4l}r(N^{3-}) - ^{[4l]}r(O^{2-}) = 0.08 \text{ \AA}$ ) is comparable to the cation size-mismatches between large  $Ba^{2+}$  or small  $Ca^{2+}$  and the dopant  $Eu^{2+}$ . Local anion clustering provides an effective way of reducing lattice strains by equalizing the mean cation–anion distances, as illustrated in Figure 4.

The  $Eu^{2+}$  dopants are larger than the host cations in the  $Ca_{1.95}Eu_{0.05}Si_{5-x}Al_xN_{8-x}O_x$  series, so lattice strain is minimized by clustering above-average numbers of oxide anions around  $Eu^{2+}$  cations (and hence more nitrides around  $Ca^{2+}$ ), as in

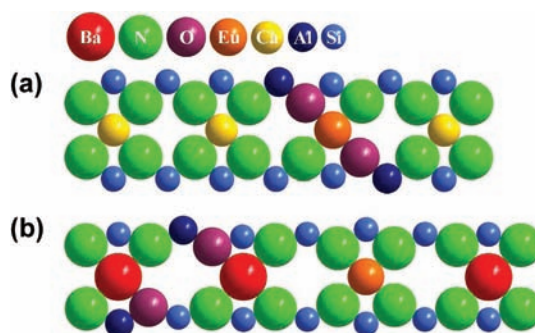


**Figure 4.** Schematic local anion distributions driven by cation size-mismatch in  $M_{1.95}Eu_{0.05}Si_{5-x}Al_xN_{8-x}O_x$  phosphors. (a) Local structure for  $Ca_{1.95}Eu_{0.05}Si_4AlN_7O$ , where  $Eu^{2+}$  is bigger than the host  $Ca^{2+}$  cations and lattice strain is minimized by clustering oxide anions around  $Eu^{2+}$  cations (and hence more nitrides around  $Ca^{2+}$ ), resulting in a blue shift of the photoluminescence. (b)  $Ba_{1.95}Eu_{0.05}Si_4AlN_7O$ , where  $Eu^{2+}$  is smaller than the host  $Ba^{2+}$  cations and so tends to be coordinated by nitride, while the introduced oxide anions preferentially coordinate  $Ba^{2+}$ .  $Al^{3+}$  is shown as preferentially coordinating oxide, consistent with the solid-state NMR spectra in Supporting Information.

Figure 4a. The increased oxide coordination around  $Eu^{2+}$  results in a large blue shift of the photoluminescence energy (Figure 2), from which the approximate coordination change may be estimated as follows. The anion coordination to each  $Ca^{2+}$  in the  $Ca_2Si_5^{[3Si]}N_4^{[2Si]}N_4$  parent structure is  $^{[2Si]}N_5^{[3Si]}N_2$ , illustrating the predominant coordination by nitrides bonded to two Si sites. Oxide substitutes only at  $^{[2Si]}N$  sites in the SiAlON derivatives, as demonstrated above by neutron diffraction (Figure 1b), so in  $Ca_{1.95}Eu_{0.05}Si_4AlN_7O$  the average  $Ca^{2+}$  and  $Eu^{2+}$  coordination is  $(^{[2Si]}N_{0.75}^{[2Si]}O_{0.25})_5^{[3Si]}N_2 = O_{1.25}N_{5.75}$ , in the absence of any anion clustering. The change from this average is estimated by assuming that the observed blue shift of  $1700 \text{ cm}^{-1}$  between the reported peak photoluminescences of  $Ca_{1.96}Eu_{0.04}Si_5N_8^{16}$  and  $Ca_{1.98}Eu_{0.02}Si_2N_2O_2^9$  results mainly from the change of  $Ca^{2+}/Eu^{2+}$  cation coordination from  $N_7$  in the former material to  $O_6N$  in the latter. Hence, by interpolation, the  $520 \text{ cm}^{-1}$  blue shift of  $Ca_{1.95}Eu_{0.05}Si_4AlN_7O$  relative to the ideal  $\Delta r = 0$  analogue (see Figure 2b) corresponds to an estimated change of  $O_{+1.85}N_{-1.85}$  in the average  $Eu^{2+}$  coordination, so although the average cation coordination in  $Ca_{1.95}Eu_{0.05}Si_4AlN_7O$  is  $O_{1.25}N_{5.75}$ , the local  $Eu^{2+}$  environment is approximately  $O_{3.1}N_{3.9}$  and the balancing  $Ca^{2+}$  coordination is  $O_{1.2}N_{5.8}$ . The change around the majority host  $Ca^{2+}$  cations is very slight, but a substantial size-driven clustering of oxides around the  $Eu^{2+}$  dopants drives the blue shift in the photoluminescence.

A reverse argument applies to predicted anion clustering in the  $Ba_{1.95}Eu_{0.05}Si_{5-x}Al_xN_{8-x}O_x$  series. Here  $Eu^{2+}$  is smaller than the host  $Ba^{2+}$  cations and so tends to be coordinated by nitride, while the introduced oxide anions preferentially coordinate  $Ba^{2+}$  as shown in Figure 4b. An estimate based on the photoluminescence shift of  $3200 \text{ cm}^{-1}$  between  $Ba_{1.96}Eu_{0.04}Si_5N_8^{16}$  and  $Ba_{1.98}Eu_{0.02}Si_2N_2O_2^9$  phosphors shows that the number of oxides coordinated to  $Eu^{2+}$  is approximately zero. Hence, for  $Ba_{1.95}Eu_{0.05}Si_4AlN_7O$ , the mean cation coordination (averaged over 8- and 10-fold sites) is  $O_{1.5}N_{7.5}$ , but the approximate local coordinations are  $N_9$  for  $Eu^{2+}$  and  $O_{1.55}N_{7.45}$  for the  $Ba^{2+}$  hosts. The red shift observed in the  $Ba_{1.95}Eu_{0.05}Si_{5-x}Al_xN_{8-x}O_x$  series thus reflects only the lattice-

expanding effect from  $\text{AlO}^+$  substitution, as the  $\text{Eu}^{2+}$  dopants are not significantly coordinated by oxide anions.

The above anion clustering model also accounts for the size-mismatch control of thermal quenching (Figure 3). Oxide phosphors are known to have lower quenching activation energies than comparable nitrides.<sup>17,18</sup> In an ideal, size-matched  $\text{M}_{1.95}\text{Eu}_{0.05}\text{Si}_{5-x}\text{Al}_x\text{N}_{8-x}\text{O}_x$  series this leads to a slight decrease in activation energy with  $x$ , illustrated by the  $\text{M} = \text{Sr}$  materials in Figure 3b, as the local  $\text{Eu}^{2+}$  coordination reflects the average anion composition. However, in the  $\text{M} = \text{Ca}$  series,  $\text{Eu}^{2+}$  ions are coordinated by substantially above-average numbers of oxides (Figure 4a), leading to a rapid decline in quenching activation energy with  $x$ . Conversely,  $\text{Eu}^{2+}$  is in a virtually pure nitride coordination environment in the  $\text{M} = \text{Ba}$  materials, despite the presence of oxides within the lattice (Figure. 4b), and the quenching activation energy increases slightly with  $x$ .

The above results show that lattice strains resulting from size-mismatch between host and dopant cations can drive large changes in the dopant coordination relative to the average in SiAlONs, even in materials synthesized at high temperatures (1600 °C for our ceramic  $\text{M}_{1.95}\text{Eu}_{0.05}\text{Si}_{5-x}\text{Al}_x\text{N}_{8-x}\text{O}_x$  samples), where entropically favored randomization might be expected to dominate the anion distributions. Minimization of local lattice strains created by cation size-mismatch results in local coordination numbers that may be far from averages based on the chemical composition or even on anion distributions from neutron diffraction. The expected number of coordinating oxides per  $\text{Eu}^{2+}$  dopant in  $\text{M}_{1.95}\text{Eu}_{0.05}\text{Si}_4\text{AlN}_7\text{O}$  lattices would be 0.9–1.1 from the chemical formula, and 1.25–1.5 based on the average anion distributions within the crystal structure. However, the coordination can increase up to  $\sim 3$  oxides per  $\text{Eu}^{2+}$  for small  $\text{M} = \text{Ca}$  host cations or decrease to  $\sim 0$  in the Ba analogue. This clustering effect provides a useful tuning of the photoluminescence wavelength by up to  $700\text{ cm}^{-1}$  relative to a size-matched reference material (here approximated by  $\text{M} = \text{Sr}$ ) and also controls the thermal quenching behavior.

The size-mismatch effect discovered in  $\text{M}_{1.95}\text{Eu}_{0.05}\text{Si}_{5-x}\text{Al}_x\text{N}_{8-x}\text{O}_x$  materials could be used to tune photoluminescence in related phosphors such as  $\alpha$ - and  $\beta$ -SiAlONs and the  $\text{MSi}_2\text{O}_2\text{N}_2$  ( $\text{M} = \text{Ca}, \text{Sr}, \text{Ba}$ ) family, and to help understand the results of combinatorial studies. Furthermore, we note that this effect should be general to cation-doped oxynitrides, including those not based on (oxo)nitridosilicate frameworks. For example, size-mismatch-driven clustering of anions may be significant in perovskite-type solid solutions in  $\text{BaTaO}_2\text{N}$ – $\text{SrTaO}_2\text{N}$  photocatalysts<sup>19</sup> and  $\text{CaTaO}_2\text{N}$ – $\text{LaTaON}_2$  red-yellow pigments,<sup>20</sup> where disordered zigzag TaN chains<sup>21</sup> may be pinned by the local cation-mismatch strains. The same effect is also expected to operate in other mixed-anion systems such as oxyfluoride ceramics and glasses, which are also important optical materials, where the anion size difference ( ${}^{[4]}r(\text{F}^-) = 1.31\text{ \AA}$ ;  ${}^{[4]}r(\text{O}^{2-}) - {}^{[4]}r(\text{F}^-) = 0.07\text{ \AA}$ ) is comparable to the  $0.08\text{ \AA}$  difference responsible for the clustering that we have observed here in oxynitride phosphors.

## ■ ASSOCIATED CONTENT

### Ⓢ Supporting Information

Experimental details; supporting figures and tables showing further crystallographic, photoluminescence, and NMR data. This material is available free of charge via the Internet at <http://pubs.acs.org>.

## ■ AUTHOR INFORMATION

### Corresponding Author

[j.p.attfield@ed.ac.uk](mailto:j.p.attfield@ed.ac.uk); [rsliu@ntu.edu.tw](mailto:rsliu@ntu.edu.tw)

### Notes

The authors declare no competing financial interest.

## ■ ACKNOWLEDGMENTS

This work was supported by EPSRC, EaStCHEM, STFC, and the Leverhulme Trust, U.K., and National Science Council of the Republic of China, Taiwan (Contract Nos. NSC 97-2113-M-002-012-MY3 and NSC 97-3114-M-002).

## ■ REFERENCES

- (1) Höpfe, H. A. *Angew. Chem., Int. Ed.* **2009**, *48*, 3572.
- (2) Setlur, A. A. *Electrochem. Soc. Interface* **2009**, *18*, 32.
- (3) Xie, R. J.; Hirosaki, N. *Sci. Technol. Adv. Mater.* **2007**, *8*, 588.
- (4) Zeuner, M.; Pagano, S.; Schnick, W. *Angew. Chem., Int. Ed.* **2011**, *50*, 7754.
- (5) He, X. H.; Lian, N.; Sun, J. H.; Guan, M. Y. *J. Mater. Sci.* **2009**, *44*, 4763.
- (6) Schlieper, T.; Milius, W.; Schnick, W. *Z. Anorg. Allg. Chem.* **1995**, *621*, 1380.
- (7) Oeckler, O.; Stadler, F.; Rosenthal, T.; Schnick, W. *Solid State Sci.* **2007**, *9*, 205.
- (8) Li, Y. Q.; van Steen, J. E. J.; van Kreveld, J. W. H.; Botty, G.; Delsing, A. C. A.; DiSalvo, F. J.; de With, G.; Hintzen, H. T. *J. Alloys Compd.* **2006**, *417*, 273.
- (9) Bachmann, V.; Ronda, C.; Oeckler, O.; Schnick, W.; Meijerink, A. *Chem. Mater.* **2009**, *21*, 316.
- (10) Mueller-Mach, R.; Mueller, G.; Krames, M. R.; Höpfe, H. A.; Stadler, F.; Schnick, W.; Juestel, T.; Schmidt, P. *Phys. Status Solidi* **2005**, *202*, 1727.
- (11) Shannon, R. D. *Acta Crystallogr.* **1976**, *A32*, 751.
- (12) Fuertes, A. *Inorg. Chem.* **2006**, *45*, 9640.
- (13) Höpfe, H. A.; Lutz, H.; Morys, P.; Schnick, W.; Seilmeier, J. *Phys. Chem. Solids* **2000**, *61*, 2001.
- (14) Piao, X.; Horikawa, T.; Hanzawa, H.; Machida, K. I. *Appl. Phys. Lett.* **2006**, *88*, 161908.
- (15) Piao, X.; Horikawa, T.; Hanzawa, H.; Machida, K. I. *Chem. Lett.* **2006**, *35*, 334.
- (16) Li, H. L.; Xie, R. J.; Hirosaki, N. *Int. J. Appl. Ceram. Technol.* **2009**, *6*, 459.
- (17) Schnick, W.; Huppertz, H. *Chem.—Eur. J.* **1997**, *3*, 679.
- (18) Piao, X.; Machida, K.; Horikawa, T.; Yun, B. *J. Lumin.* **2010**, *130*, 8.
- (19) Pors, F.; Bacher, P.; Marchand, R.; Laurent, Y.; Roult, G. *Rev. Int. Hautes Tempér. Réfract* **1988**, *24*, 239.
- (20) Jansen, M.; Letschert, H. P. *Nature* **2000**, *404*, 980.
- (21) Yang, M.; Oró-Solé, J.; Rodgers, J. A.; Jorge, A. B.; Fuertes, A.; Attfield, J. P. *Nature Chem.* **2011**, *3*, 47.

## ■ NOTE ADDED AFTER ASAP PUBLICATION

This paper was published ASAP on April 27, 2012, with an incomplete References list and errors in some of the citations. The corrected version was reposted on May 2, 2012.